

# Instabilities in a two-dimensional polar filament–motor system

Victor Rühle<sup>a</sup>, Falko Ziebert<sup>b</sup>, Ronny Peter and Walter Zimmermann<sup>c</sup>

Theoretische Physik, Universität Bayreuth, D-95440 Bayreuth, Germany

Received: date / Revised version: date

**Abstract.** The dynamical interaction between filaments and motor proteins is known for their propensity to selforganize into spatiotemporal patterns. Since the filaments are polar in the sense that motors define a direction of motion on them, motors might induce, under certain conditions, a spatially homogeneous polar filament orientation. We show that the latter two-dimensional anisotropic state itself may become unstable with respect to inhomogeneous fluctuations. This scenario shares similarities with instabilities in planarly aligned nematic liquid crystals since the wave vector of the instabilities may be oriented in both cases either parallel or oblique to the polarity axis. However, the encountered instabilities are long-wave instead of short-wave and the destabilizing modes are drifting ones due to the polar filament orientation. The instability becomes nonpropagating in case of the wave vector perpendicular to the polarity. The resulting phase diagrams of the instabilities related to various wave vector orientations relative to the polarity axis are determined and discussed for a specific model of motor-filament interactions.

**PACS.** 87.16.-b Subcellular structure – 47.54.+r Pattern formation – 89.75.-k Complex systems

## 1 Introduction

Cell organization relies on the collective behavior of a large variety of macromolecules. A prominent example, the cytoskeleton, consists of semiflexible actin filaments, the more rigid microtubules, as well as motor and cross-linker proteins which interconnect the polymers dynamically or permanently, respectively [1–3]. The latter ingredients define a material class with very interesting and not yet fully explored features - be it structural, mechanical, dynamical or rheological ones. Apart from the more global aspects of e.g. cell mechanics, the collective and dynamical interactions in the presence of the biological fuel adenosine triphosphate (ATP) may result in dissipative structures [4–7]. Examples are mitosis and cell locomotion, where spindle and fiber structures emerge [8,9].

In order to principally understand cellular dynamics it is thus worthwhile to explore the various kinds of patterns and instabilities that might be encountered in a cytoskeletal solution of interacting filaments and motor proteins. A number of in vitro experiments revealed different types of self-organization phenomena induced by motor–filament interactions [10–14]. In most of these quasi two-dimensional experiments the initial state is a homogeneous and isotropic distribution of filaments and motor proteins.

<sup>a</sup> *Present address:* Max Planck Institute for Polymer Research, Ackermannweg 10, 55128 Mainz, Germany.

<sup>b</sup> *Present address:* Materials Science Division, Argonne National Laboratory, 9700 South Cass Avenue, Argonne, IL 60439, USA.

<sup>c</sup> e-mail: [walter.zimmermann@uni-bayreuth.de](mailto:walter.zimmermann@uni-bayreuth.de)

A diversity of spatio-temporal patterns may evolve from such a highly symmetric basic state, a number of them being found in two-dimensional models and simulations as well [13–20]. Furthermore it is well known that microtubules [21] and actin filaments [22] exhibit anisotropic states due to orientational order provided that the filament density is high enough. This ordering transition is related to the fact that excluded volume interaction is more costly than the loss in entropy due to the ordering [23] and seems to become even more probable in a nonequilibrium case where active motors are present [24, 25].

The question, which kind of spatio-temporal patterns may emerge from such an anisotropic basic state naturally arises. Both actin filaments and microtubules are *polar* as molecular motors move on them only in one direction. The polar character is also apparent in the polymerization kinetics of these filaments. The aforesaid structural polarity, i.e. distinguishable filament ends, hence defines head and tail or plus and minus ends of a filament. Consequently there are two different homogeneous anisotropic basic states: If the anisotropy originates predominantly from excluded volume effects, as in lyotropic liquid crystalline (LC) systems, the orientation of the filament heads is on average equally distributed in both directions of the axial anisotropy, giving the sample nematic character [26]. However, if the filaments are actively oriented by motors it is very likely that the basic state is a *polar* anisotropic one, for which there is strong evidence, both in vitro [27] and from simulations [28].

In the present work we determine within a common two-dimensional model the range of parameters wherein the anisotropic polar state becomes unstable against inhomogeneous fluctuations. In contrast to previous studies [16, 29, 18], starting from a homogeneous and isotropic state, the question to ask here is how the perturbation wave vector is oriented with respect to the axial anisotropy: Will the wave vector of the most unstable mode be longitudinal, perpendicular or oblique with respect to the preferred direction?

Investigations on pattern forming instabilities in two-dimensional physical systems with an axial anisotropy have some tradition [26, 30–33, 5]. The two most prominent physical examples belonging to this class are electroconvection and Rayleigh-Bénard convection in planarly oriented nematic LCs [26]. Comparable patterns can occur in active media close to the isotropic-nematic transition as well [34]. The aforesaid physical examples are studied for over three decades and associated spatially periodic dissipative patterns have been evinced experimentally by applying to a planarly oriented layer of a nematic LC either an AC electric field in the case of electroconvection or a thermal gradient in the case of thermal convection. For some time, in nematic LCs only spatially periodic patterns have been observed with their wave vectors parallel to the preferred molecular mean orientation. Later on it has been found experimentally and theoretically [35–38] that convection rolls may emerge in these systems with their wave vectors obliquely oriented with respect to the direction of the nematic ordering. The continuous transition from the so-called normal rolls to the oblique roll state happens at the so-called Lifshitz-point [39, 37, 38]. Additionally, in polymeric LCs a static instability characterized by a wave vector perpendicular to the preferred nematic orientation has been found [40, 41].

Since the system at hand presents a *polar* anisotropy yielding a broken  $\pm$ -symmetry along the anisotropy axis, the patterns with the wave vector parallel to the anisotropy are propagating ones. In contrast to travelling structures triggered by a Hopf-bifurcation [5], the propagating patterns encountered in the analysed system always drift in a specific direction determined by the polarity. The eigenvalues of these drifting patterns are therefore not complex conjugated as will be seen in section 4. This still holds for an obliquely oriented pattern, whereas the patterns with the preferred wave vector perpendicular to the anisotropy are stationary. All instabilities, whether longitudinal, perpendicular or oblique, are long-wavelength instabilities arising from the competition of the conserved filament density and the broken-symmetry mode of the orientation. Thus they share similarities with decomposition phenomena with respect to the unstable long-wavelength modes, the rotational and reflexion symmetries along the axis of the preferred direction being however broken in the present case. The respective equations covering the essential features close to the transition points therefore belong to different symmetry classes than in LCs and are extended versions of the famous Cahn-Hilliard equation [42], which will be discussed elsewhere [43].

This work is organized as follows: The model for the filament distribution, taking active motor-mediated currents into account, has already been described in the literature [16, 18] and is therefore only briefly summarized in section 2, with some details given in appendix A in order to remain self-contained. The full nonlinear equations for the density and the orientation field of the filaments obtained by a coarse-graining procedure detailed in Ref. [18], can be read from appendix A.2. However they are not crucial in their entirety to understand the main body of this work: in section 3 we determine the motor-induced homogeneous, polar basic state given by the homogeneous part of the equations and in section 4 we discuss the linearized equations governing the dynamics of the linear perturbations with respect to the basic state. The phase diagrams for the various instabilities are presented in section 5 and the work is concluded with a discussion and outlook in section 6.

## 2 Model

Since the model used to describe the filament-motor-system has been discussed and explored to quite some extent during recent years [16, 44, 29, 18, 24, 45, 46, 14], its formulation is kept short and we refer for more details to Refs. [16, 18, 45] and to appendix A. The starting point is a Smoluchowski equation [47],

$$\partial_t \Psi + \nabla \cdot \mathbf{J}_t + \mathcal{R} \cdot \mathbf{J}_r = 0, \quad (1)$$

capturing the evolution of the probability density function (pdf)  $\Psi(\mathbf{r}, \mathbf{u}, t)$  of finding a rigid filament at the position  $\mathbf{r}$  with orientation  $\mathbf{u}$  (with  $|\mathbf{u}| = 1$ ) at a given time  $t$ . Both, the translational and the rotational current,  $\mathbf{J}_t$  and  $\mathbf{J}_r$  respectively, have the well known passive contributions from diffusion and excluded volume interaction [47], given in the appendix by Eqs. (27) and (28). The active (nonpotential) contributions induced by homogeneously distributed motors are given by the following two expressions

$$\mathbf{J}_t^a = \Psi \int d\mathbf{u}' \int d\mathbf{r}' \mathbf{v}(\mathbf{r}-\mathbf{r}', \mathbf{u}, \mathbf{u}') W(\mathbf{r}-\mathbf{r}', \mathbf{u}, \mathbf{u}') \Psi', \quad (2)$$

$$\mathbf{J}_r^a = \Psi \int d\mathbf{u}' \int d\mathbf{r}' \boldsymbol{\omega}(\mathbf{u}, \mathbf{u}') W(\mathbf{r}-\mathbf{r}', \mathbf{u}, \mathbf{u}') \Psi', \quad (3)$$

with  $\Psi = \Psi(\mathbf{r}, \mathbf{u})$  and  $\Psi' = \Psi(\mathbf{r}', \mathbf{u}')$ . Its structure can be understood as follows: upon overlap of two filaments, with coordinates  $(\mathbf{r}, \mathbf{u})$  and  $(\mathbf{r}', \mathbf{u}')$ , a motor exerts on this filament pair a relative velocity  $\mathbf{v}$  and angular velocity  $\boldsymbol{\omega}$ . Up to the leading order these velocities read

$$\mathbf{v}(\mathbf{r}-\mathbf{r}', \mathbf{u}, \mathbf{u}') = \frac{\alpha}{2} \frac{\mathbf{r}' - \mathbf{r}}{L} \frac{1 + \mathbf{u} \cdot \mathbf{u}'}{|\mathbf{u} \times \mathbf{u}'|} + \frac{\beta}{2} \frac{\mathbf{u}' - \mathbf{u}}{|\mathbf{u} \times \mathbf{u}'|}, \quad (4)$$

$$\boldsymbol{\omega}(\mathbf{u}, \mathbf{u}') = \gamma_0 \frac{\mathbf{u} \times \mathbf{u}'}{|\mathbf{u} \times \mathbf{u}'|} + \gamma_1 (\mathbf{u} \cdot \mathbf{u}') \frac{\mathbf{u} \times \mathbf{u}'}{|\mathbf{u} \times \mathbf{u}'|}. \quad (5)$$

This specific form of the active motor contributions has been suggested in Ref. [16], while modifications have been

discussed in Refs. [29,24]. The above active currents fulfill both the conservation of translational and rotational momentum in the absence of external forces and torques, as well as translational and rotational invariance [16,18].

In the one-dimensional limit of the model, the  $\alpha$ -contribution in Eq. (4) reflects, as anticipated in Ref. [48], the interaction of parallel filaments whereas the  $\beta$ -contribution accounts for the interaction of anti-parallel ones. The  $\beta$  term is responsible for a process called *polarity sorting* [10,49,50] that induces a maximum antiparallel filament separation and thus favors an arrangement with regions of alternating local polarities.

In Ref. [18] the model with only the motor-interaction of parallel filaments, i.e. with the active translational current proportional to  $\alpha$ , has been analyzed. This reduced motor-filament model already displayed nontrivial stationary density-orientation patterns with finite wavelength. It has also been shown that the  $\gamma_1$ -contribution to the active rotational current only slightly affects the stability regions of these patterns. The  $\gamma_0$ -contribution to the active rotational current however changes the universality class of the model by introducing a new nontrivial symmetry-broken basic state: if this term is large enough to overcome rotational diffusion, it can trigger a homogeneously polarized state. The importance of motor-induced filament rotations has been pointed out in Ref. [19]. Polar phases are also currently discussed from a more macroscopic point of view [17,51]. In the present work we investigate the stability of the homogeneously polarized state induced by the  $\gamma_0$ -contribution as a function of the motor parameters  $\alpha$  and  $\beta$ . For the sake of simplicity we use  $\gamma_1 = 0$ , which has no influence on the qualitative instability behavior of the polar state. It has been shown, however, that increasing  $\gamma_1$  decreases the threshold of the isotropic-nematic transition [24].

The model at hand is defined through the conservation law Eq. (1) with the entering currents given by Eqs. (27) and (28) of appendix A with the active contributions from Eqs. (2) and (3) and the relative translational and angular velocities Eqs. (4) and (5). Eq. (1) then becomes a rather complicated nonlinear integro-differential equation for the pdf  $\Psi(\mathbf{r}, \mathbf{u}, t)$ . However, upon approximating the nonlocal interactions by a gradient expansion, equations for the zeroth, the first and the second moment with respect to the orientation, can be derived by a moment expansion technique. The moments of interest are the filament density  $\rho(\mathbf{r}, t)$ , the polar orientation  $\mathbf{t}(\mathbf{r}, t)$  and the nematic order parameter  $S_{ij}(\mathbf{r}, t)$  as defined by the following expressions

$$\begin{aligned}\rho(\mathbf{r}, t) &= \int d\mathbf{u} \Psi(\mathbf{r}, \mathbf{u}, t) , \\ \mathbf{t}(\mathbf{r}, t) &= \int d\mathbf{u} \mathbf{u} \Psi(\mathbf{r}, \mathbf{u}, t) , \\ S_{ij}(\mathbf{r}, t) &= \int d\mathbf{u} u_i u_j \Psi(\mathbf{r}, \mathbf{u}, t) .\end{aligned}\quad (6)$$

Details on both the gradient and the moment expansion can be found in Ref. [18].

We should stress that in contrast to a usual, passive lyotropic LC, as described by the Onsager theory [23],

the herein considered filaments are *polar* with respect to the motor action: motors can walk on filaments only in one motor specific direction defined by the internal protein structure of both the motor and the filament. This unidirectionality of motion breaks the  $\pm\mathbf{u}$ -symmetry and allows the first moment, namely  $\mathbf{t}(\mathbf{r}, t)$ , to become non-vanishing in motor-filament systems. In the absence of motor-mediated filament-rotations,  $\gamma = 0$ , it has been demonstrated in Ref. [18], that a polar orientation occurs only locally in connection with spatially variations of the filament density.

Provided that the system is in a polarized state and that the filament density is small compared to the critical density at the isotropic-nematic transition, the nematic order is most likely to be slaved to the polar vector [51]. Thus the nematic order parameter does not give rise to an additional degree of freedom but plays nevertheless a role in stabilizing the growth of the polar orientation. This allows for the nematic order parameter to be adiabatically eliminated, leading to a stabilizing term in the equation of the polar orientation as detailed in appendix B.

Ultimately, in two spatial dimensions, one obtains a system of three coupled nonlinear equations for the filament density  $\rho$  and the two components of the polar orientation field  $t_i$  ( $i = x, y$ ) of the filaments. The complete nonlinear equations can be found in appendix A.2 while for the following only the homogeneous parts as well as the linear operator will be important. The structure of the equations is as follows

$$\begin{aligned}\partial_t \rho &= \partial_j f_j, \\ \partial_t t_i &= -D_r t_i + \frac{\gamma_0}{2} \rho t_i + \partial_j g_{ij} + \frac{A}{2} t_j t_j t_i .\end{aligned}\quad (7)$$

The equation for the density, Eq. (7), is a conservation law with  $f_j$  being a function of both the density, the orientation and gradients thereof as well as of the motor parameters  $\alpha$  and  $\beta$ . Both rotational diffusion and active rotations, namely the contributions including  $D_r$  or  $\gamma_0$ , are not present in the equation for the scalar density field. The equations for the polar field, cf. Eq. (8), have a conserved part mainly due to translational motion of the filaments (with  $g_{ij}$  in contrast to  $f_j$  now being a function of  $D_r$  and  $\gamma_0$  as well), but also homogeneous contributions related to rotational diffusion and motor-induced filament rotations. The term proportional to  $A$ , with

$$A = \frac{\gamma_0 \left( \frac{8D_r}{3\pi} - \gamma_0 \right)}{4D_r \left( 1 - \frac{2}{3\pi} \rho_0 \right)}, \quad (9)$$

results for  $A < 0$  in a stabilizing term for the polar orientation. This term is due to the nematic order being slaved to the orientation field (see appendix B).

We should mention that for convenience, throughout this work we use rescaled variables for time and space,  $t' = t(D_{\parallel}/L^2)$ ,  $x' = x/L$ , filament density and orientation field,  $\rho' = \rho/L^2$ ,  $\mathbf{t}' = \mathbf{t}/L^2$ , for the motor interaction parameters,  $\alpha' = \alpha(L/D_{\parallel})$ ,  $\beta' = \beta(L/D_{\parallel})$ ,  $\gamma'_0 = \gamma_0(L^2/D_{\parallel})$ , and the rotational diffusion coefficient,  $D'_r = D_r(L^2/D_{\parallel})$ , as well as having introduced the ratio of the two translational diffusion coefficients,  $D = D_{\perp}/D_{\parallel}$ .

### 3 Homogeneous polar state

As discussed above, the motor parameter  $\gamma_0$  describes active motor-induced rotations of a filament pair and can therefore lead to a homogeneous polar state. This transition from a homogeneous isotropic filament distribution to a homogeneous polarized state is governed by the homogeneous part of Eq. (8),

$$\partial_t t_i = -(D_r - \frac{\gamma_0}{2}\rho_0)t_i + \frac{A}{2}t_j t_j t_i, \quad (10)$$

with the homogeneous filament density  $\rho_0$ . Eq. (10) immediately yields that for

$$\gamma_0 > \gamma_0^* = \frac{2D_r}{\rho_0} \quad (11)$$

the isotropic filament distribution, corresponding to  $\mathbf{t} = 0$ , gets unstable with respect to small perturbations  $\delta t_i$ . As within the regions of occurrence of polar states  $A < 0$ , the associated growth finally saturates due to the cubic term at a value

$$\bar{t} = \sqrt{\frac{\gamma_0 \rho_0 - 2D_r}{-A}}. \quad (12)$$

When discussing the stability of the latter polar state, only a linearization around such a stationary solution of the basic equations, given by  $\bar{\mathbf{t}} = \bar{t} \hat{\mathbf{t}}$  with  $\hat{\mathbf{t}}$  being the unit vector of an arbitrary direction, gives the correct answer to the stability of the polar state. In contrast to prior work [45], a state with finite and constant polar order  $\mathbf{t}$  should not be assumed a priori since the saturation of the polar order affects the stability and perturbations of the modulus of the polar order have to be taken into account.

### 4 Stability of the homogeneous polar state

The two-dimensional homogeneous, polar state determined in the previous section may become unstable with respect to small inhomogeneous perturbations. The direction of the basic polar state is chosen to be the  $x$ -axis, thus the polarity of the basic state is described by

$$\bar{\mathbf{t}} = (\bar{t}, 0), \quad (13)$$

which we call the polarity axis. The equations of the perturbations around this state are obtained from the fundamental model equations by separating the homogeneous polarity and filament density from inhomogeneous contributions by the ansatz

$$\begin{pmatrix} \rho \\ t_x \\ t_y \end{pmatrix} = \begin{pmatrix} \rho_0 \\ \bar{t} \\ 0 \end{pmatrix} + \begin{pmatrix} \delta \rho \\ \delta t_x \\ \delta t_y \end{pmatrix}. \quad (14)$$

A linearization of the basic equations with respect to the small perturbations  $\delta \rho$ ,  $\delta t_x$  and  $\delta t_y$  then yields three coupled equations with constant coefficients that may be written as follows,

$$\partial_t \mathbf{w}(\mathbf{r}, t) = \mathcal{L} \mathbf{w}(\mathbf{r}, t), \quad (15)$$

with  $\mathbf{w}$  denoting the vector  $\mathbf{w} = (\delta \rho, \delta t_x, \delta t_y)$ . The linear operator  $\mathcal{L} = \mathcal{L}^\rho + \mathcal{L}^t$  consists of the isotropic components  $\mathcal{L}^\rho$  that arise when linearizing  $\rho = \rho_0 + \delta \rho$  around  $\rho_0$  while the components  $\mathcal{L}^t$  are due to the linearization of  $\mathbf{t} = \bar{\mathbf{t}} + \delta \mathbf{t}$ . The contribution  $\mathcal{L}^t$  renders the equations anisotropic and is purely due to the intrinsic anisotropy. The explicit components of the rotational invariant operator  $\mathcal{L}^\rho$  are

$$\begin{aligned} \mathcal{L}_{11}^\rho &= \left[ \frac{1+D}{2} \left( 1 + \frac{2}{\pi} \rho_0 \right) - \frac{\alpha \rho_0}{24} \right] \Delta - \frac{19}{11520} \frac{\alpha \rho_0}{\Delta^2}, \\ \mathcal{L}_{12}^\rho &= -\frac{\beta}{96} \frac{5}{2} \rho_0 \Delta \partial_x, \quad \mathcal{L}_{13}^\rho = -\frac{\beta}{96} \frac{5}{2} \rho_0 \Delta \partial_y, \\ \mathcal{L}_{21}^\rho &= \left\{ \frac{\beta \rho_0}{2} + \frac{\beta}{96} \frac{5}{4} \rho_0 \Delta \right\} \partial_x, \\ \mathcal{L}_{22}^\rho &= -D_r + \frac{3D+1}{4} \Delta + \frac{1-D}{2} \partial_x^2 - \frac{\alpha \rho_0}{96} (\Delta + 2\partial_x^2) \\ &\quad - \frac{\alpha \rho_0}{46080} (11\Delta^2 + 64\Delta \partial_x^2) + \frac{\gamma_0}{2} \rho_0 + \frac{\gamma_0 \rho_0}{48} \Delta, \\ \mathcal{L}_{23}^\rho &= \left( \frac{1-D}{2} - \frac{\alpha \rho_0}{48} \right) \partial_x \partial_y - \frac{\alpha \rho_0}{720} \Delta \partial_x \partial_y, \\ \mathcal{L}_{31}^\rho &= \left\{ \frac{\beta \rho_0}{2} + \frac{\beta}{96} \frac{5}{4} \rho_0 \Delta \right\} \partial_y, \quad \mathcal{L}_{32}^\rho = \mathcal{L}_{23}^\rho, \\ \mathcal{L}_{33}^\rho &= -D_r + \frac{3D+1}{4} \Delta + \frac{1-D}{2} \partial_y^2 - \frac{\alpha \rho_0}{96} (\Delta + 2\partial_y^2) \\ &\quad - \frac{\alpha \rho_0}{46080} (11\Delta^2 + 64\Delta \partial_y^2) + \frac{\gamma_0}{2} \rho_0 + \frac{\gamma_0 \rho_0}{48} \Delta \end{aligned} \quad (16)$$

and the anisotropic operator contributions read

$$\begin{aligned} \mathcal{L}_{11}^t &= \frac{5\beta}{192} \bar{t} \Delta \partial_x, \\ \mathcal{L}_{12}^t &= -\frac{\alpha}{48} \bar{t} (\Delta + 2\partial_x^2) - \frac{\alpha}{23040} \bar{t} (11\Delta^2 + 64\Delta \partial_x^2), \\ \mathcal{L}_{13}^t &= -\frac{\alpha}{24} \bar{t} \partial_x \partial_y - \frac{\alpha}{360} \bar{t} \Delta \partial_x \partial_y, \\ \mathcal{L}_{21}^t &= \frac{3D+1}{2\pi} \bar{t} \Delta + \frac{1-D}{\pi} \bar{t} \partial_x^2 - \frac{\alpha}{96} \bar{t} (3\Delta + 2\partial_x^2) \\ &\quad - \frac{\alpha}{11520} \bar{t} (11\Delta^2 + 16\Delta \partial_x^2) + \frac{\gamma_0}{2} \bar{t}, \\ \mathcal{L}_{22}^t &= -\beta \bar{t} \partial_x - \frac{\beta}{96} \bar{t} (2\Delta \partial_x + \partial_x^3) + \frac{3A}{2} \bar{t}^2, \\ \mathcal{L}_{23}^t &= -\frac{\beta}{2} \bar{t} \partial_y - \frac{\beta}{96} \bar{t} (2\Delta \partial_y + \partial_x^2 \partial_y), \\ \mathcal{L}_{31}^t &= \left[ \frac{1-D}{\pi} - \frac{\alpha}{48} \right] \bar{t} \partial_x \partial_y - \frac{\alpha}{720} \bar{t} \Delta \partial_x \partial_y, \\ \mathcal{L}_{32}^t &= -\frac{\beta}{96} \bar{t} \partial_x^2 \partial_y, \\ \mathcal{L}_{33}^t &= -\frac{\beta}{2} \bar{t} \partial_x - \frac{\beta}{96} \bar{t} \partial_x \partial_y^2 + \frac{A}{2} \bar{t}^2. \end{aligned} \quad (17)$$

The coupled system of linear equations with constant coefficients (15) is solved by the ansatz

$$\mathbf{w} = \mathbf{A} \exp(\sigma t + i\mathbf{k} \cdot \mathbf{r}) \quad (18)$$

with wave vector  $\mathbf{k} = (k_x, k_y)$  and the corresponding eigenvector  $\mathbf{A}$ . For the studied anisotropic system the interesting question is whether the orientation of the wave vector

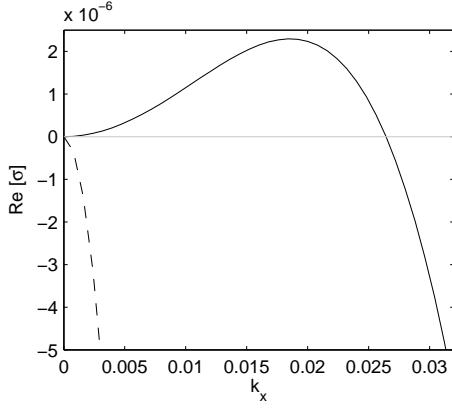


**Fig. 1.** Dependence of the growth rates of the eigenvalue with the largest real part (solid line) and with the second largest real part (dashed line) on the wavenumber  $k_x$  ( $k_y = 0$ ).

corresponding to the largest growth rate  $\text{Re}[\sigma]$  is parallel, oblique or perpendicular to the polarity axis  $\bar{\mathbf{t}} = (\bar{t}, 0)$ .

Numerical solution of the eigenvalue problem reveals that the typical wavenumber dependence of the two eigenvalues with largest real part is always of the form depicted in Fig. 1, wherein both are shown as a function of the wavenumber  $k_x$  in the case of a longitudinal instability. Hence the instabilities are always long-wavelength ones which makes a Taylor expansion of the eigenvalues with respect to small values of the wavenumber  $k$  suitable. If we choose accordingly an expansion up to third order in  $k$

$$\sigma = i\omega(\varphi)k + \lambda(\varphi)k^2 + i\nu(\varphi)k^3 + \dots \quad (19)$$

with  $k_x = k \cos(\varphi)$ ,  $k_y = k \sin(\varphi)$ , we get two approximated long-wave eigenvalues:

$$\begin{aligned} \sigma_1 = & \left[ \left( \frac{\rho_0}{12} - \frac{\gamma_0}{96A} \right) \alpha - (1+D) \left( \frac{\rho_0}{\pi} - \frac{1}{2} \right) \right. \\ & \left. - \left( \frac{\gamma_0}{48A} + \frac{\rho_0}{24} \right) \cos^2 \varphi \right] k^2 \\ & + i\nu_1 k^3 + \mathcal{O}(k^4), \end{aligned} \quad (20)$$

with  $\nu_1 \neq 0$  and

$$\begin{aligned} \sigma_2 = & -ik \frac{\beta}{2} t_0 \cos \varphi + \left[ -\frac{3+D}{4} - \frac{\gamma_0 + 2\alpha}{48} \rho_0 \right. \\ & \left. + \left( \frac{1-D}{2} + \frac{\alpha\rho_0}{48} \right) \cos^2 \varphi \right] k^2 + i\nu_2 k^3 + \mathcal{O}(k^4) \end{aligned} \quad (21)$$

within the range  $0 \leq \varphi < \pi/2 - \epsilon$  (see below) with  $\nu_2 \neq 0$ . For the relevant parameter ranges,  $\sigma_1$  is always governing the onset of instability while  $\sigma_2$  is damped.

In the limit of transverse perturbations, for which  $\varphi = \pi/2$  holds, the latter two equations reduce to

$$\sigma_{1,2}^{(y)} = \left( -b \pm \sqrt{b^2 - 4c} \right) k^2 \in \mathbb{R} \quad (22)$$

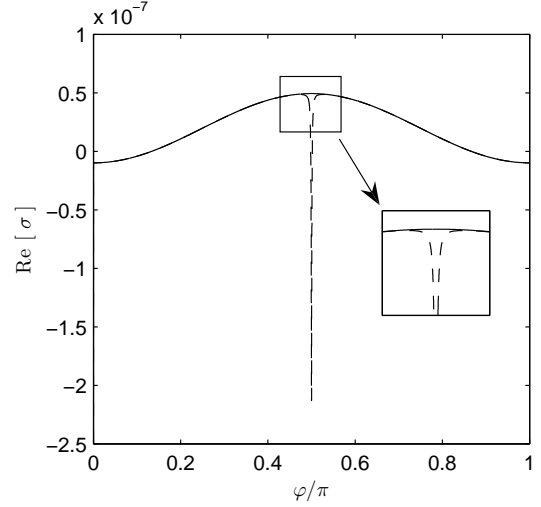


**Fig. 2.** Comparison between the analytical growth rates (solid line) gained by the Taylor series Eq. (19) and the numerics of the full third order dispersion relation (dashed line) for the parameters  $\rho_0 = 0.5$ ,  $D = D_r = 0.5$ ,  $\alpha = 20.5$ ,  $\beta = 2$  and  $\gamma_0 = 2.5$  at  $k = 10^{-3}$ . Up to a small neighborhood of  $\varphi = \pi/2$ , the expansion Eq. (19) is a good approximation.

wherein the abbreviations

$$\begin{aligned} b = & \frac{1}{48} \gamma_0 \rho_0 + \frac{1+D}{\pi} \rho_0 + \frac{\gamma_0 \alpha}{96A} + \frac{5+3D}{4} - \frac{7}{96} \rho_0 \alpha, \quad (23) \\ c = & \frac{2\rho_0 + \pi}{8\pi} \left[ (D+2)^2 - 1 \right] + \frac{\alpha\gamma_0}{384A} (D+3) \\ & + \frac{\alpha\rho_0}{9216} (3\alpha - 2\gamma_0) (3\rho_0 - \gamma_0) \\ & + \frac{\rho_0 \beta^2}{384A} (5\rho_0 A + 2\alpha) - \frac{\alpha\rho_0}{192} (5D+9) \\ & + \frac{D+1}{96} (\gamma_0 \rho_0 + 2\gamma_0 \rho_0^2 + 3\alpha \rho_0^2) \end{aligned} \quad (24)$$

have been introduced. Eqs. (20) and (21) clearly evince that the growth rates  $\text{Re}[\sigma_i]$  of the perturbations depend on the angle  $\varphi$  enclosed by the wave vector  $\mathbf{k}$  and the polarity axis. The considered system being anisotropic, the wave vector of the critical mode can be parallel, perpendicular or even oblique to the axis of polarity. As the polarity  $\bar{\mathbf{t}}$  breaks furthermore the systems reflexion symmetry along this direction, the emerging patterns of either longitudinal or oblique character are drifting ones, according to the finite imaginary parts of the eigenvalues  $\sigma_{1,2}$ , while the eigenvalues  $\sigma^y$  of the transverse modes are real.

The angle  $\varphi$  for which the growth rate's curvature changes its sign for the first time will be referred to as the critical angle  $\varphi_c$ . This angle is in general different from the one enclosed by the wave vector  $\mathbf{k}$  corresponding to the maximum of  $\sigma(\mathbf{k}) > 0$  and the polarity. As shown in Fig. 2, in the neighborhood of  $\varphi = \pi/2$  the growth behavior of the unstable modes is not fully covered by the Taylor expansion: to estimate the validity of the power series Eq. (19), the analytical growth rates are compared to the numerically obtained full third order dispersion re-

lation for a specific parameter set. The analytical results are in good agreement with the numerics for any angle  $\varphi$  up to the critical one close to  $\varphi = \varphi^* \lesssim \pi/2$ , with  $\varphi^*$  in the immediate vicinity of the maximum of the solid line in Fig. 2.

## 5 Stability diagrams

In two-dimensional extended systems the wave number-dependent growth rate, depicted in Fig. 1 along the  $k_x$  direction, is a function of both  $k_x$  and  $k_y$ . In the current section it will be shown that the location of the maximum of the growth rate  $\text{Re}[\sigma(k_x, k_y)]$  as well as the critical angle  $\varphi_c$  strongly depend on the parameters of the motor-filament interactions. At first we will discuss the possible generic instability scenarios and subsequently present the related phase diagrams.

For a filament density of  $\rho_0 = 0.5$  and diffusion coefficients  $D = D_r = 0.5$ , Figs. 3 and 4 visualize the three generic instability cases. In Fig. 3a) the contour lines  $\text{Re}[\sigma(k_x, k_y)] = \text{const.}$  are shown for the motor-related parameters  $\alpha = 18.5$ ,  $\beta = 2$  and  $\gamma_0 = 2.1 > \gamma_0^*$ . For this parameter set, the function  $\text{Re}[\sigma(k_x, k_y)]$  has its maximum at a finite value of  $k_x$  while  $k_y = 0$ . The corresponding instability is therefore a longitudinal one, characterized by a critical angle  $\varphi_c = 0$ . Alternatively,  $\text{Re}[\sigma(k_x, k_y)]$  can take its maximum at finite  $k_y$  and vanishing  $k_x = 0$ , as shown in Fig. 3b) for  $\alpha = 19$ ,  $\beta = 5$  and  $\gamma_0 = 2.5 > \gamma_0^*$ . The associated instability is transverse with the critical angle  $\varphi_c$  being  $\pi/2$ .

Interestingly the third typical instability, exemplified for  $\alpha = 20.5$ ,  $\beta = 2$ ,  $\gamma_0 = 2.5 > \gamma_0^*$  in Fig. 4, simultaneously breaks the translational symmetry both along the  $x$ - and the  $y$ -axis. The maximum of the growth rate is situated at finite values of  $k_x \neq 0$  and  $k_y \neq 0$  and we refer to this scenario as an *oblique* instability because the critical angle  $\varphi_c$  lies within the interval  $]0, \pi/2[$ , analogous to instabilities in usual (i.e. apolar and passive) nematic LCs leading to the so-called oblique rolls [35–38]

The rich instability scenario found in this system is best studied as a function of the two motor transport parameters  $\alpha$  and  $\beta$ , as well as of the motor-induced rotation parameter  $\gamma_0$ . If one of the transport parameters exceeds a certain critical threshold value, the homogeneous polar state becomes unstable as can be seen in Fig. 5 for two different values of the motor parameter  $\gamma_0$  which evaluates in part a) to  $\gamma_0 = 2.1$  while in b)  $\gamma_0 = 2.5$ . As previously the chosen values of  $\rho_0$  and  $D_r$  satisfy in both cases the relation  $\gamma_0 > \gamma_0^*$  which accordingly makes the homogeneous state a polar one.

Since the occurring instabilities are long-wavelength ones, the critical values of the parameters  $\alpha$  and  $\beta$  can be calculated from the change of sign of the angle dependent growth rate at  $\mathbf{k} = 0$ , namely

$$d^2 \text{Re}[\sigma(k, \varphi)] / dk^2 \Big|_{k=0} = \lambda(\varphi). \quad (25)$$

In case of a longitudinal or oblique instability the  $\beta$ -independent critical value of the motor parameter  $\alpha$  can be

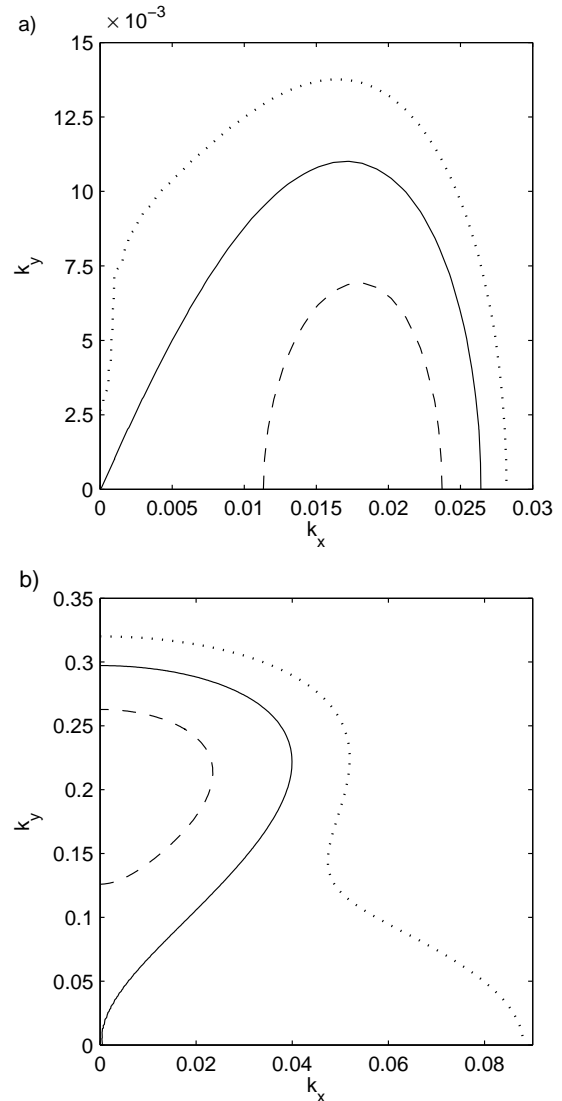


**Fig. 3.** The contour lines  $\text{Re}[\sigma(k_x, k_y)] = \text{const.}$  of the eigenvalue with the largest real part are shown for three different values of const. In part a) the growth rate has its maximum at a finite value of  $k_x \neq 0$  and  $k_y = 0$ . Contour lines correspond to  $\text{Re}[\sigma(k_x, k_y)] = 0$  (solid line),  $1.4 \cdot 10^{-6}$  (dashed line) and  $-1.4 \cdot 10^{-6}$  (dotted line). Part b) shows a growth rate taking its maximum at a finite value of  $k_y \neq 0$  while  $k_x = 0$ . Contour lines:  $\text{Re}[\sigma(k_x, k_y)] = 0$  (solid line),  $10^{-3}$  (dashed line) and  $-10^{-3}$  (dotted line).

obtained by substituting  $\sigma_1$  from Eq. (20) into Eq. (25),

$$\alpha_c = \frac{(1+D) \left( \frac{\rho_0}{\pi} + \frac{1}{2} \right) + \left( \frac{\gamma_0}{48A} + \frac{\rho_0}{24} \right) \cos^2 \varphi}{\left( \frac{\rho_0}{12} - \frac{\gamma_0}{96A} \right)}. \quad (26)$$

When inserting  $\varphi = 0$ , Eq. (26) defines the threshold of the longitudinal instability while a possible onset value of the oblique instability is yielded for  $0 < \varphi \leq \varphi^* \lesssim \pi/2$ . If the term proportional to  $\cos^2 \varphi$  is positive (as is the case for Fig. 5b), the threshold of the oblique instability is lower

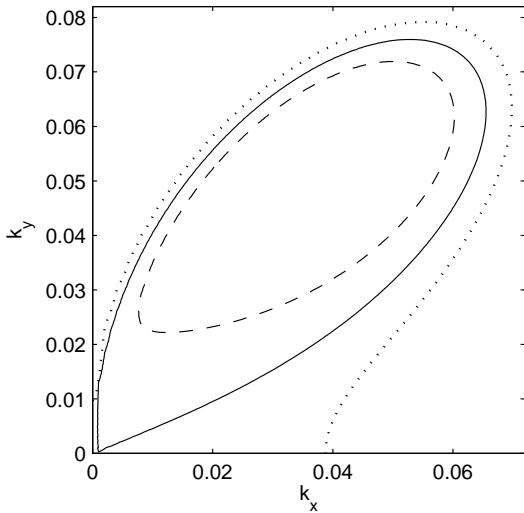


**Fig. 4.** Similarly to Fig. 3, the contour lines of the largest growth rate are visualized in the case of an oblique instability. The maximum is located at nonvanishing  $k_x$  and  $k_y$ . The contour lines correspond to  $\text{Re}(\sigma(k_x, k_y)) = 0$  (solid line),  $10^{-3}$  (dashed line) and  $-10^{-3}$  (dotted line).

than the onset of the longitudinal one. The onset criterion for the oblique instability derived from Eq. (26) at  $\varphi = \varphi^* \lesssim \frac{\pi}{2}$  defines however only the smallest possible onset value that is not necessarily realised. The actual critical control parameter value  $\alpha_c$  triggering the emergence of an oblique instability can not be calculated analytically as it does depend on the motor parameter  $\beta$  not present in the approximated growth rate Eq. (20).

The onset of the longitudinal instability corresponds to the vertical solid lines in Fig. 5a) and b), while the dotted line in Fig. 5b) visualizes the possible onset value of the oblique instability at  $\varphi = \varphi^* \lesssim \frac{\pi}{2}$ . In case of Fig. 5a) this line lies beyond the longitudinal threshold and therefore is irrelevant. The dash-dotted line in Fig. 5b) corresponds to the numerically obtained exact value of the oblique instability threshold (see above). If  $\alpha$  is below the thresholds of the longitudinal and oblique instabilities, an increase of the motor parameter  $\beta$  results in the transverse instability beyond the dashed lines in Fig. 5a) and b), gained by using Eq. (25) with  $\sigma = \sigma_1^{(y)}$  from Eq. (22).

Instead of studying a large variety of phase diagrams comparable to those shown in Fig. 5 by varying the ratio  $\gamma_0/D_r$ , it is beneficial to fix the motor parameter  $\alpha$  to its critical value  $\alpha_c(\beta, \gamma_0/D_r)$  in order to get a phase diagram  $\beta$  versus the ratio  $\gamma_0/D_r$ . Fig. 6 highlights which instability type dominates when  $\alpha$  approaches the instability threshold. The area of the  $\beta$ - $\gamma_0/D_r$  plane labelled I, located below the left solid line at  $\gamma_0/D_r = 4$  corresponds to the stability region of the isotropic state for which the motor-induced rotations are not sufficient to generate a polar state, cf. Eq. (11). To the right of the right solid line the adiabatic elimination of the nematic order parameter fails to yield saturation of the polar order. In between the latter two domains, upon increasing the motor parameter

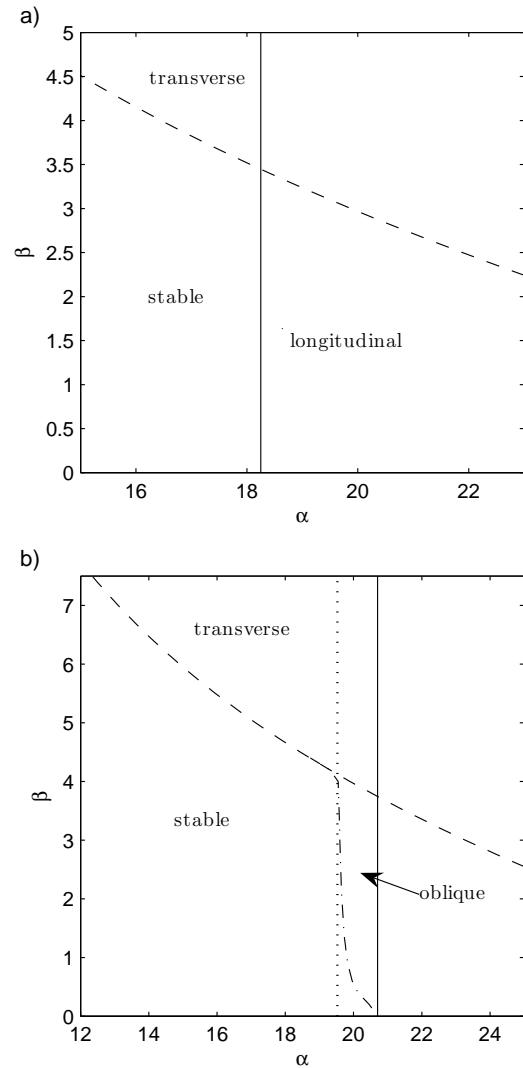


**Fig. 5.** Two typical phase diagrams show the ranges within the  $\alpha$ - $\beta$  plane where the polar state is either stable or unstable against a longitudinal, transverse or oblique instability. In part a)  $\gamma_0 = 2.1$  holds whereas in part b)  $\gamma_0 = 2.5$ , with the remaining parameters  $\rho_0 = 0.5$ ,  $D = D_r = 0.5$ . The solid line governs the transition to the longitudinal instability given by the analytical formula, Eq. (26) with  $\varphi = 0$ . The dotted line corresponds to the possible threshold value of the oblique instability yielded by Eq. (26) for  $\varphi = \frac{\pi}{2}$ , which is smaller than the longitudinal threshold in case b). The transition to a transverse instability takes place at the dashed line obtained from Eq. (22). The dash-dotted line in part b) is the exact, numerically obtained threshold to patterns bifurcating from the homogeneous polar state.

$\alpha$ , the polar basic state becomes either unstable to the longitudinal, the transverse or to the oblique instability.

The transition from the longitudinal to an oblique instability setting in at the dashed line in Fig. 6 requires the prefactor of  $\cos^2 \varphi$  in Eq. (26) to change its sign, that is when  $\gamma_0 + 2A\rho = 0$ . The dotted line claims that the curvature  $d^2 \text{Re}[\sigma_1^{(y)}]/dk^2$  of the transversal instability as well

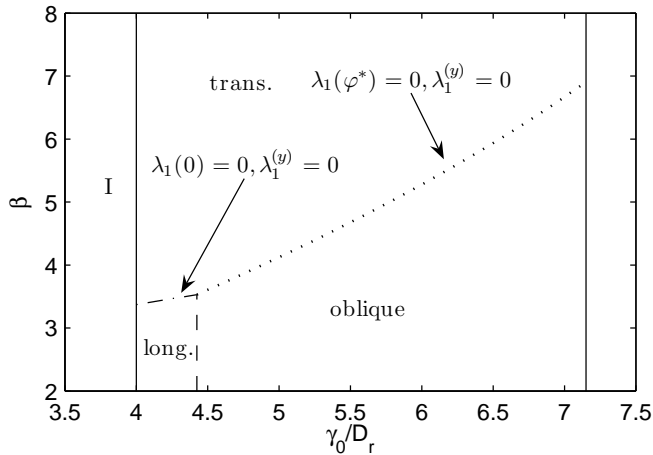


**Fig. 6.** This phase diagram shows for  $\rho_0 = 0.5$  and  $D = D_r = 0.5$  the parameter ranges wherein the homogeneous polar state becomes unstable with respect to modes having their wave vector either longitudinal, oblique or transverse to the anisotropy axis. In region I the system is isotropic, whereas to the right of the right solid line the adiabatic elimination is not valid anymore.

as the curvature  $d^2\text{Re}[\sigma_1(\varphi \lesssim \pi/2)]/dk^2$  of the oblique instability change simultaneously their sign and is thus gained from the codimension-2 condition,  $d^2\text{Re}[\sigma_1^{(y)}]/dk^2 = d^2\text{Re}[\sigma_1(\varphi = \varphi^*)]/dk^2 = 0$ . Accordingly the function  $\lambda(\varphi)$  has for parameters along the dash-dotted line zeroes at  $\varphi = 0, \pi/2$  and is otherwise negative in between. In another scenario the curvature of transverse and longitudinal instability change their signs simultaneously. This is the case along the dash-dotted line in Fig. 6 which is determined by  $d^2\text{Re}[\sigma_1^{(y)}]/dk^2 = d^2\text{Re}[\sigma_1(\varphi = 0)]/dk^2 = 0$ . Along these borders interesting nonlinear pattern competition is expected. Although the boundaries of the oblique instability are approximated by the choice  $\varphi = \varphi^* \lesssim \pi/2$ , both the dotted and the dash-dotted line are well confirmed by numerical calculations.

As indicated in Fig. 6 the longitudinal and the oblique instability occur only for small values of  $\beta$ . An interesting question is how the transition from the longitudinal to the oblique instability takes place. If the motor parameter  $\alpha$  is again presumed to evaluate to its critical value, Fig. 7 shows this transition in the  $\gamma_0/D_r$ - $\rho_0$ -plane. The dash-dotted line is the transition point from longitudinal to oblique instability. Underneath the solid line the isotropic state persists whereas above the dashed line the approximative adiabatic elimination of the nematic order parameter fails.

Besides the regions of occurrence of the diverse instabilities, the critical angle  $\varphi_c$  for whom the curvature changes its sign and which is enclosed by the wave vector and the polarity axis, is a relevant observable in case of an oblique instability. For the model at hand  $\varphi_c$  is varying as a function of the filament density  $\rho_0$  and the ratio  $\gamma_0/D_r$ . In case of a filament density  $\rho_0 = 0.5$ , the latter angle is shown in Fig. 8 as a function of  $\gamma_0/D_r$  for three

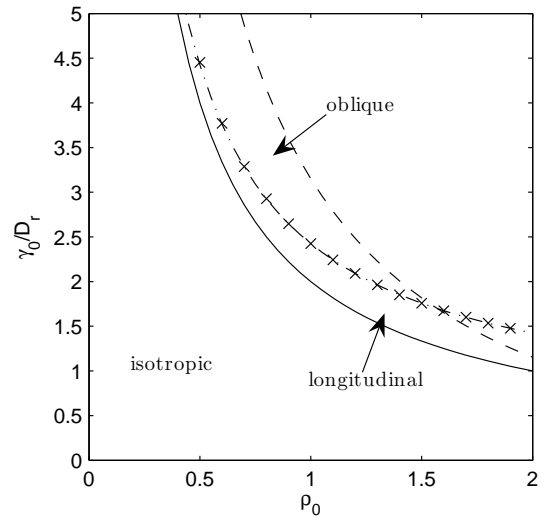


**Fig. 7.** In between the solid and the dashed line, the homogeneous polar state is unstable with respect to either longitudinal or oblique modes. The dash-dotted curve, at which the transition from longitudinal to oblique instability sets in, is obtained from the condition  $\gamma_0 + A\rho = 0$ , while crosses show the numerically obtained threshold. Underneath the solid line the system is isotropic while above the dashed line the approximation of adiabatic elimination fails.

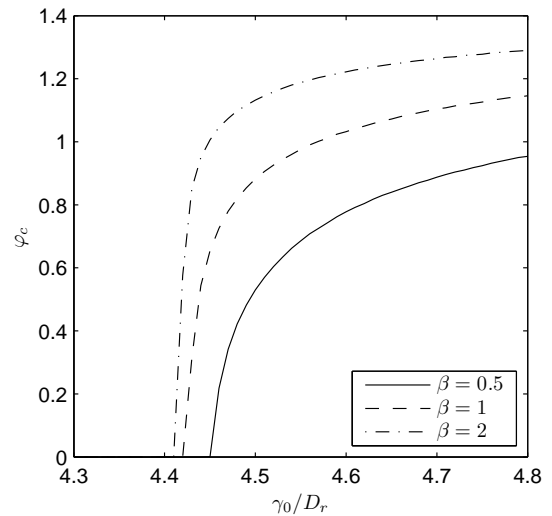


**Fig. 8.** The numerically determined critical angle  $\varphi_c$  is shown as a function of the ratio  $\gamma_0/D_r$  for a given filament density  $\rho_0 = 0.5$  and for three different values of  $\beta$ .

different values of the motor transport parameter  $\beta$ . This figure clearly evinces, that the transition from the longitudinal to the oblique instability is a continuous one. Nevertheless, it may be deduced that the angle increases from  $\varphi = 0$  very steeply at a critical  $\gamma_0$ , which favors experimental observations of the oblique instability as a finite angle should be easily distinguishable from the transverse and longitudinal instability scenario.

## 6 Conclusion

In this work pattern forming instabilities have been analyzed that occur in a standard model for motor-filament systems and evolve from a homogeneous polar filament state. Hitherto only instabilities emerging from a homogeneous isotropic distribution of filaments have been discussed in detail [16,44,18]. Within a certain parameter range, however, one finds a homogeneous polar filament order, which breaks the systems rotational symmetry. This anisotropic polar filament state may itself become unstable upon increasing the filament density or/and upon increasing the motor activity with respect to long-wavelength perturbations similarly to various kinds of decomposition phenomena and in contrast to finite-wavelength instabilities occurring for an isotropic state.

The systems anisotropy causes another difference to former filament-motor studies. Depending on the model parameters, the wave vector  $\mathbf{k} = (k_x, k_y)$  at the maximum of the perturbation growth rate  $\text{Re}[\sigma(k_x, k_y)]$  as well as the critical one are oriented either longitudinally, perpendicularly or even obliquely to the polarity axis. This is in contrast to Ref. [45], where the only primary instability found was one with the wave vector parallel to the anisotropy.

The encountered instability types additionally break the systems translational symmetry along the distinguished axes: in case of the longitudinal instability, the translational symmetry along the polarity axis is broken, whereas for a transverse instability, it is violated along the perpendicular direction. For an oblique instability, translational symmetry is no longer fulfilled in both spatial directions. The parameter ranges, wherein the transverse and oblique instabilities are preferred, happen to be significantly broader than those wherein the longitudinal instability is favored. According to the broken  $x \rightarrow -x$  symmetry along the polar direction the unstable longitudinally and obliquely oriented modes will be nonstationary and drifting. Only the transverse instability remains nonpropagating. Varying appropriate model parameters triggers a continuous transition from a longitudinal to an oblique instability as for instance along the vertical dashed line in Fig. 6. Since this transition is continuous, as indicated in Fig. 8, it shares some similarities with the so-called Lifshitz point identified with the transition from a longitudinal finite wavenumber instability to an oblique one in electroconvection of planarly aligned nematic LCs [32,35,37,38]. There are nevertheless two utterly important differences between pattern forming systems with an axial anisotropy, such as electroconvection and Rayleigh-Bénard convection in planarly aligned LCs, and instabilities emerging from the polar state of an interacting motor-filament system. In case of nematic LCs the instability's growth rate is damped at small wavenumbers and only modes at finite wavenumbers are likely to grow. For filament-motor systems, finite wavenumber instabilities also occur evolving from the isotropic basic state as discussed in [18]. The instabilities building up from a polar state, however, are always long-wavelength within the considered standard model. Additionally, due to the po-

larity and the broken  $x \rightarrow -x$  symmetry the unstable modes of the polar state have to be drifting in contrast to nematic LCs where the bifurcations are either stationary with the eigenvalue's imaginary part vanishing or oscillatory, meaning one has a Hopf-bifurcation characterized by a pair of complex conjugated eigenvalues.

As the nonlinear evolution of the unstable modes is concerned, finite wavelength instabilities in planarly aligned nematic LCs belong to the universality class of pattern forming systems with axial anisotropy, while two-dimensional and rotational symmetric pattern forming systems, such as thermal convection in simple fluids, are members of a different universality class. It is well established that, due to the different symmetries, the slow dynamics of the long-wavelength modulated patterns are described near onset of pattern formation in terms of different generic and symmetry adapted envelope equations [5]. Thus the aforesaid amplitude equations differ for Rayleigh-Bénard convection in simple fluids [52,53] and electroconvection in planarly aligned nematic LCs [39,37,32]. In case of the bifurcations met in motor-filaments systems, when starting from the isotropic state, the generic envelope equations capturing the slow pattern dynamics in the weakly nonlinear regime have been derived and solved in Ref. [18], belonging to the symmetry class of two-dimensional, rotationally symmetric systems like thermal convection. The patterns considered in the present work however, bifurcating from a polar state, are governed by envelope equations falling into a symmetry class not corresponding to either of the cases mentioned above. The long-wavelength nature of the instabilities predicted in this work together with the broken  $\pm$ -symmetry in the polarity direction requires new types of generic equations as will be reported elsewhere [43].

For selected parameter sets the investigated model equations have already been solved numerically for each of the instability types presented in the current work. While these preliminary simulations show rather spatiotemporal chaos than coarsening dynamics if the chosen parameter set falls into the predicted domain of longitudinal or oblique instability, the transverse instability gives rise to the formation of parallel filament bundles. A thorough nonlinear analysis will be provided elsewhere.

### Acknowledgments

This work has been supported by a grant from the Deutsche Forschungsgemeinschaft via research unit FOR 608. R. P. acknowledges a fellowship from the BioMedTec International Graduate School of Science (BIGSS), supported by the state of Bavaria.

## A Details of the mesoscopic model

### A.1 Currents

The continuity of the probability expressed by Eq. (1) involves a translational and a rotational current. The former,

$$J_{t,i} = -D_{ij} [\partial_j \Psi + \Psi \partial_j V_{ex}] + J_{t,i}^a, \quad (27)$$

contains besides anisotropic diffusion and an excluded volume potential  $V_{ex}$ , arising from the other filaments in the solution, the active contribution  $\mathbf{J}_t^a$  caused by the molecular motors, as defined in the main body. The rod-like shape of the filaments additionally motivates a rotational current,

$$J_{r,i} = -D_r [\mathcal{R}_i \Psi + \Psi \mathcal{R}_i V_{ex}] + J_{r,i}^a, \quad (28)$$

with a structure analogous to the translational current except that the anisotropic diffusion matrix,

$$D_{ij} = D_{\parallel} u_i u_j + D_{\perp} (\delta_{ij} - u_i u_j) \quad (29)$$

with parallel and perpendicular diffusion coefficients,  $D_{\parallel}$  and  $D_{\perp}$  respectively, is replaced by the rotational diffusion coefficient  $D_r$  and the spatial derivatives are replaced by the operator of rotational diffusion [47],  $\mathcal{R} = \mathbf{u} \times \partial_{\mathbf{u}}$ . The excluded volume interaction,

$$V_{ex}(\mathbf{r}, \mathbf{u}) = \int d\mathbf{u}' \int d\mathbf{r}' W(\mathbf{r}-\mathbf{r}', \mathbf{u}, \mathbf{u}') \Psi(\mathbf{r}', \mathbf{u}') , \quad (30)$$

is governed by the interaction kernel  $W(\mathbf{r}-\mathbf{r}', \mathbf{u}, \mathbf{u}')$ , which evaluates to 1 if there is an overlap of the filaments at  $(\mathbf{r}, \mathbf{u})$  and  $(\mathbf{r}', \mathbf{u}')$  and to zero otherwise.

## A.2 Nonlinear equations

Performing a gradient expansion and extracting equations of motion for the moments of the orientation distribution from Eq. (1), as detailed in Ref. [18], the two-dimensional nonlinear equations for the density  $\rho$  and the orientation field  $\mathbf{t} = (t_x, t_y)$  read (in the rescaled variables as defined above)

$$\begin{aligned} \partial_t \rho = & \frac{1+D}{2} \Delta \rho + \left[ \frac{1+D}{\pi} - \frac{\alpha}{24} \right] \nabla \cdot (\rho \nabla \rho) \\ & - \frac{\alpha}{48} \partial_i \left[ t_i \partial_j t_j + t_j \partial_i t_j + t_j \partial_j t_i \right] \\ & - \frac{\alpha}{23040} \left\{ 38 \nabla \cdot (\rho \nabla \Delta \rho) + 11 \partial_i (t_j \partial_i \Delta t_j) \right. \\ & \quad \left. + 16 \partial_i \left[ t_i \Delta \partial_j t_j + 2 t_j \partial_j \partial_i \partial_t t_l + t_j \partial_j \Delta t_i \right] \right\} \\ & - \frac{\beta}{96} \partial_i \left[ \rho \partial_i \partial_j t_j - t_j \partial_j \partial_i \rho + \frac{3}{2} (\rho \Delta t_i - t_i \Delta \rho) \right], \quad (31a) \end{aligned}$$

$$\begin{aligned} \partial_t t_i = & -D_r t_i + \frac{3D+1}{4} \Delta t_i + \frac{1-D}{2} \partial_i \nabla \cdot \mathbf{t} \\ & + \frac{3D+1}{2\pi} \partial_j (t_i \partial_j \rho) + \frac{1-D}{2\pi} \left[ (\partial_j (t_j \partial_i \rho) + \partial_i (t_j \partial_j \rho)) \right] \\ & - \frac{\alpha}{96} \partial_j \left[ 3 t_i \partial_j \rho + t_j \partial_i \rho + \rho (\partial_i t_j + \partial_j t_i) \right] \\ & - \frac{\alpha}{96} \partial_i \left[ t_l \partial_l \rho + \rho \partial_t t_l \right] - \frac{16\alpha}{46080} \partial_i \left[ \rho \Delta \partial_t t_l + t_l \partial_l \Delta \rho \right] \\ & - \frac{\alpha}{46080} \partial_j \left[ \rho \left( 11 \partial_j \Delta t_i + 16 \partial_i \Delta t_j + 32 \partial_j \partial_i \partial_t t_l \right) \right. \\ & \quad \left. + 16 t_j \partial_i \Delta \rho + 32 t_l \partial_l \partial_i \partial_j \rho + 44 t_i \partial_j \Delta \rho \right] \\ & + \frac{\beta}{2} \partial_j \left[ \frac{1}{2} \delta_{ij} \rho^2 - t_i t_j \right] + \frac{\beta}{96} \partial_j \left[ \frac{3}{4} \delta_{ij} \rho \Delta \rho + \frac{1}{2} \rho \partial_i \partial_j \rho \right] \\ & - \frac{\beta}{96} \partial_j \left[ t_l \partial_l \partial_i t_j + t_i \partial_j \partial_l t_l + t_i \Delta t_j \right] \\ & + \frac{\gamma_0}{2} \rho t_i + \frac{\gamma_0}{48} \rho \Delta t_i + \frac{A}{2} t_j t_j t_i . \quad (31b) \end{aligned}$$

## B Stabilizing term for the polar state

As discussed above, for high enough  $\gamma_0$  the isotropic basic state becomes unstable against a polar ordered state. The growth of this polar orientation needs to be stabilized by higher order nonlinearities. As a rigorous treatment of the nematic order parameter would be cumbersome and gives rise to additional equations, here we will motivate the stabilizing term used in Eq. (31). The homogeneous equations for the polar orientation and the nematic order parameter read

$$\partial_t t_i = - \left( D_r - \frac{\gamma_0 \rho}{2} \right) t_i + \left( \frac{8}{3\pi} D_r - \gamma_0 \right) S_{ij} t_j, \quad (32)$$

$$\begin{aligned} \partial_t S_{ij} = & -4D_r \left( 1 - \frac{2}{3\pi} \rho_0 \right) S_{ij} + \gamma_0 \left( t_i t_j - \frac{1}{2} \delta_{ij} t^2 \right) \\ & + \frac{32}{9\pi} D_r \left( S_{im} S_{jm} - \frac{1}{2} \delta_{ij} S_{lm}^2 \right). \quad (33) \end{aligned}$$

Provided that  $\gamma_0 > \gamma^* = 2D_r/\rho_0$  the polar orientation gets unstable and has to be stabilized (within the approximations used so far) by the nonlinear term proportional to  $S_{ij} t_j$ . The equation for  $S_{ij}$ , Eq. (33), stipulates that for  $\rho > \frac{3\pi}{2}$  a transition to a nematic phase takes place. However, as only parameter ranges lying beneath the nematic transition point are considered here, equations governing the spatiotemporal evolution of the filament density and polar orientation should be sufficient to describe the systems behavior. Furtheron one can assume that below the nematic transition point, the polar orientation and the nematic order parameter are strongly coupled yielding for  $S_{ij}$  the subsequent form [47]

$$S_{ij} = \tilde{S} \left( t_i t_j - \frac{1}{2} \delta_{ij} t^2 \right). \quad (34)$$

In order for  $S_{ij}$  to be consistent with the definition in Eq.(6), the relation  $0 \leq S_0 \leq \rho_0$  needs to hold. Presuming that the nematic order follows the polar order adiabatically, i.e.  $\partial_t S_{ij} = 0$ , one gets from Eq. (34) and Eq. (33)

$$\tilde{S} = \frac{\gamma_0}{4D_r \left(1 - \frac{2}{3\pi}\rho\right)}. \quad (35)$$

Eliminating  $S_{ij}$  from Eq. (32) finally yields

$$\partial_t t_i = - \left( D_r - \frac{\gamma_0 \rho}{2} \right) t_i + \frac{A}{2} t_j^2 t_i \quad (36)$$

with the desired cubic term proportional to

$$A = \frac{\gamma_0 \left( \frac{8D_r}{3\pi} - \gamma_0 \right)}{4D_r \left( 1 - \frac{2}{3\pi}\rho_0 \right)}. \quad (37)$$

## References

1. B. Alberts *et al.*, *Molecular Biology of the Cell* (Garland Publishing, New York, 2001).
2. J. Howard, *Mechanics of Motor Proteins and the Cytoskeleton* (Sinauer, Sunderland, 2001).
3. H. Lodish *et al.*, *Molecular Cell Biology* (W.H. Freeman, New York, 2004).
4. A. Turing, Phil. Trans. R. Soc. London B **237**, 37 (1952).
5. M. C. Cross and P. C. Hohenberg, Rev. Mod. Phys. **65**, 851 (1993).
6. A. J. Koch and H. Meinhardt, Rev. Mod. Phys. **66**, 1481 (1994).
7. J. D. Murray, *Mathematical Biology I and II* (Springer, Berlin, 2003).
8. E. Karsenti and I. Vernos, Science **294**, 543 (2001).
9. E. Karsenti, F. Nédélec, and T. Surrey, Nature Cell Biology **8**, 1204 (2006).
10. K. Takiguchi, J. Biochem. **109**, 502 (1991).
11. R. Urrutia *et al.*, Proc. Natl. Acad. Sci. USA **88**, 6701 (1991).
12. F. Nédélec, T. Surrey, A. Maggs, and S. Leibler, Nature **389**, 305 (1997).
13. T. Surrey, F. Nédélec, S. Leibler, and E. Karsenti, Science **292**, 116 (2001).
14. D. Smith *et al.*, Molecular motor-induced instabilities and crosslinkers determine biopolymer organization, Biophys. J., in press (2007).
15. F. Nédélec, J. Cell Bio. **158**, 1005 (2002).
16. T. Liverpool and M. Marchetti, Phys. Rev. Lett. **90**, 138102 (2003).
17. K. Kruse *et al.*, Eur. Phys. J. E **16**, 5 (2005).
18. F. Ziebert and W. Zimmermann, Eur. Phys. J. **18**, 41 (2005).
19. I. S. Aranson and L. S. Tsimring, Phys. Rev. E **71**, 050901 (2005).
20. I. S. Aranson and L. S. Tsimring, Phys. Rev. E **74**, 031915 (2006).
21. A. L. Hitt, A. R. Cross, and J. R. C. Williams, J. Bio. Chem. **265**, 1639 (1990).
22. A. Suzuki, T. Maeda, and T. Ito, Biophys. J. **59**, 25 (1991).
23. L. Onsager, Ann. N.Y. Acad. Sci. **51**, 627 (1949).
24. A. Ahmadi, T. B. Liverpool, and M. C. Marchetti, Phys. Rev. E **72**, 060901(R) (2005).
25. P. Kraikivski, R. Lipowsky, and J. Kierfeld, Phys. Rev. Lett. **96**, 258103 (2006).
26. P. G. de Gennes and J. Prost, *The Physics of Liquid Crystals* (Clarendon, Oxford, 1993).
27. A. B. Verkhovskiy, T. M. Svitkina, and G. G. Borisy, Curr. Bio. **9**, 11 (1998).
28. F. Ziebert and I. S. Aranson, Rheological and structural properties of active filament solutions, submitted to Phys. Rev. Lett., 2007.
29. T. B. Liverpool and M. C. Marchetti, Europhys. Lett. **69**, 846 (2005).
30. L. Kramer *et al.*, Liquid Crystals **5**, 699 (1989).
31. S. Kai and W. Zimmermann, Prog. Theor. Phys. Suppl. **99**, 458 (1989).
32. L. Kramer and W. Pesch, Ann. Rev. Fluid Mech. **27**, 515 (1995).
33. A. Buka and L. Kramer, *Pattern Formation in Liquid Crystals* (Springer, Berlin, 1996).
34. F. Ziebert and W. Zimmermann, Phys. Rev. E **70**, 022902 (2004).
35. W. Zimmermann and L. Kramer, Phys. Rev. Lett. **55**, 402 (1985).
36. R. Ribotta, A. Joets, and L. Lei, Phys. Rev. Lett. **56**, 1595 (1986).
37. E. Bodenschatz, W. Zimmermann, and L. Kramer, J. Phys. **49**, 1875 (1988).
38. W. Thom, W. Zimmermann, and L. Kramer, Liquid Crystals **4**, 309 (1989).
39. W. Pesch and L. Kramer, Z. Physik. B **63**, 121 (1986).
40. F. Lonberg and R. B. Meyer, Phys. Rev. Lett. **55**, 718 (1985).
41. W. Zimmermann and L. Kramer, Phys. Rev. Lett. **56**, 2656 (1985).
42. J. W. Cahn and J. E. Hilliard, J. Chem. Phys. **28**, 258 (1958).
43. R. Peter, V. Rühle, F. Ziebert, and W. Zimmermann, in preparation, 2007.
44. F. Ziebert and W. Zimmermann, Phys. Rev. Lett. **93**, 159801 (2004).
45. A. Ahmadi, M. C. Marchetti, and T. B. Liverpool, Phys. Rev. E **74**, 061913 (2006).
46. F. Ziebert, M. Hammele, and W. Zimmermann, Nonl. Phenomena in Complex Systems **9**, 198 (2006).
47. M. Doi and S. F. Edwards, *The Theory of Polymer Dynamics* (Clarendon Press, Oxford, 1986).
48. K. Kruse and F. Jülicher, Phys. Rev. Lett. **85**, 1778 (2000).
49. H. Nakazawa and K. Sekimoto, J. Phys. Soc. Japan **65**, 2404 (1996).
50. A. B. Verkhovskiy, T. M. Svitkina, and G. G. Borisy, J. Cell Sci. **110**, 1693 (1997).
51. H. R. Brand, H. Pleiner, and F. Ziebert, Phys. Rev. E **74**, 021713 (2006).
52. A. C. Newell and J. A. Whitehead, J. Fluid Mech. **38**, 279 (1969).
53. A. C. Newell, T. Passot, and J. Lega, Ann. Rev. Fluid Mech. **25**, 399 (1992).